Efficient mm-wave photomodulation via coupled Fabry-Perot cavities

L. E. Barr,[1, a)] I. R. Hooper,[1] S. M. Hornett,[1] C. R. Lawrence,[2] and E. Hendry[1]
[1)]*Department of Physics and Astronomy, University of Exeter, Exeter, EX4 4QL, UK*
[2)]*QinetiQ, Cody Technology Park, Ively Road, Farnborough, GU14 0LX, UK*

(Dated: 18 January 2021)

An efficient mm-wave photomodulator is designed based on coupled Fabry-Perot modes in a low-lifetime silicon wafer and an adjacent cavity formed from a transparent reflector, such as indium tin oxide. The modulation of a reflected beam using this coupled-cavity design is increased by a factor of 7 compared with that from an isolated silicon wafer, while also introducing a degree of tunability and maintaining low angular dispersion. For the particular design built and tested, a modulation of 32% is achieved for an extremely low optical illumination of just 0.006 W/cm^2, and with a maximum operation rate of more than 3 kHz. The large increase in modulation, coupled with the flexibility of the design and the fact that all components can be industrially manufactured, make this photomodulator a promising candidate for many communication, imaging and sensing applications.

I. INTRODUCTION

Efficient modulators for THz and mm-wave radiation could open the door to a range of real-world applications in this challenging yet advantageous frequency regime. Applications already investigated include gas detection[1], biomedical imaging[2,3] and ultra-high-bandwidth communication networks[4,5]. While much progress has been made in this area in recent years, many of these technologies have yet to reach commercial application. This is primarily due to the challenge of creating cheap and efficient components for THz and mm-wave frequencies. Dynamic elements such as modulators are particularly important and challenging.

From the range of potential modulator inputs, we choose to focus on all-optical modulation, rather than thermally driven modulation, which tends to be limited in speed[6], or electrically induced modulation, which is difficult to implement in spatial modulators[7–10]. All-optical modulators are relatively simple to implement, have the potential for fast switching, and can operate over a wide range of frequencies[11]. They are also easily addressable, can encode spatial information and can be employed for complex tasks such as imaging[2,12]. These photomodulators typically consist of a photoconductive material, such as silicon, which increases in conductivity upon optical illumination as charge carriers are excited into the conduction band. In order to achieve the large modulations necessary, intense optical sources are often needed, which has curtailed the use of this technology outside the research laboratory[12]. In an effort to avoid this, much recent work has looked for ways to improve the efficiency of THz and mm-wave photomodulators.

Table 1 contains a summary of photomodulators from recent literature. To aid comparison, we introduce a modulation figure of merit (FoM) as the ratio between the percentage modulation and the optical intensity required to achieve this in W/cm^2. The maximum modulation rate is also given for comparison, and a brief description of the design. The modulators that achieve a large modulation FoM are usually severely limited in modulation rate[13,14] as they rely on photoactive materials with long charge carrier lifetimes. Other approaches tend to restrict the bandwidth[15,16] and offer no easy route for tuning the frequency, or involve complex fabrication[17,18] or modulator geometries[19,20]. In this work we exploit coupled Fabry-Perot (FP) cavity modes to increase the photomodulation of a silicon wafer with a charge carrier lifetime that is significantly lower than the intrinsic bulk lifetime, thus producing a simple, fast and efficient photomodulator with low angular dispersion that is tunable across a broad frequency range.

II. SILICON PHOTOMODULATOR DESIGN

We begin by studying the modulation obtained from a single silicon wafer in isolation. We define the modulation of a reflected beam, M_R, as the difference in the reflected intensity when the silicon is dark, R_dark, and illuminated, $R_\mathrm{illuminated}$: $M_\mathrm{R} = R_\mathrm{dark} - R_\mathrm{illuminated}$. Similarly the modulation of a transmitted beam is $M_\mathrm{T} = T_\mathrm{dark} - T_\mathrm{illuminated}$. We have chosen a definition of modulation that is not normalised in order to avoid misleadingly large modulations in cases where the dark reflection is low.

We assume that the charge carrier concentration, Δn is uniform across the wafer, which has been shown to be a reasonable approximation[13]. This can be described by the equation,

$$\Delta n = \frac{\tau_\mathrm{eff} G}{d}, \tag{1}$$

where τ_eff is the effective lifetime of the charge carriers, G is the generation rate of the carriers, which is proportional to the intensity of the photoexciting light, and d is the thickness of the silicon wafer. From Eqn. 1 it is clear that thin wafers with high charge carrier lifetimes under strong optical illumination will result in large carrier densities, and thus large modulation. However, there is a limit as to how thin a perfect, crystalline, defect-free wafer of silicon can be grown while still being robust. There is also a need to avoid intense optical illumination, as this requires powerful pulsed lasers which are not

[a)]Electronic mail: l.barr@exeter.ac.uk

TABLE I. Summary of photomodulators taken from the literature, compared to the photomodulator designed in this work. *FoM calculated using absorbed pump power instead of total incident power.

Reference	Modulation FoM (% per W/cm^2)	Modulation Rate	Design feature
This work	*5333*	*3 kHz*	*Coupled Fabry-Perot cavities, tunable between 120 - 180 GHz*
Hooper 2019[13]	90000	125 Hz	Silicon cavity with charged passivation layer, at frequency of 67 GHz
Li 2020[14]	419	4 MHz	Photo-conducting layer of YAG:Ce on silicon, for frequencies 0.2 - 1.8 THz
Wen 2014[21]	369	200 kHz	Graphene layer on germanium substrate, for frequencies 0.25 - 1 THz
Liu 2016[19]	210	—	Silicon wafer in total internal reflection, for frequencies 150 - 600 GHz
Wen 2020[17]	93.8	100 kHz	Array of silicon micro-pyramids, for frequencies 0.3 - 1 THz
Wen 2019[18]	57	>100 Hz	Islands of silicon with gold nanoparticle coating, for frequencies 0.2 - 1.2 THz
Born 2014[16]	124*	<1 kHz	Wire grid applied to silicon cavity, at frequency of 942 GHz
Chen 2014[15]	618	$\sim$ 1.6 kHz	1D photonic crystal made of silicon with air defect, at frequency of 336 GHz

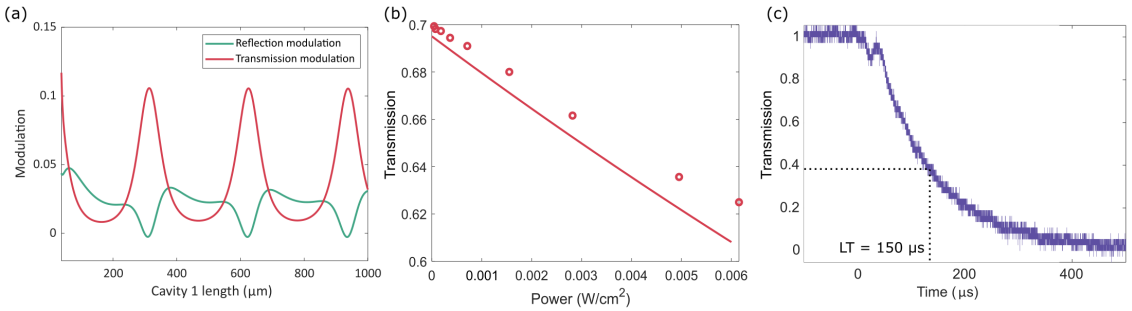

FIG. 1. (a) Simulated modulation of a normally incident 140 GHz beam reflected from (green) and transmitted through (red) a silicon wafer with a charge carrier lifetime of 150μs, as a function of the length of cavity 1, the wafer thickness. The pump beam has a wavelength of 623 nm and an intensity of 0.006 W/cm^2. (b) Experimental (circles) and calculated (solid line) transmission of a 140 GHz beam incident at 45° on a 290μm thick silicon wafer as a function of the intensity of illumination of the pump beam. (c) Measurement of the transmission upon switching on the pump beam as a function of time, showing that the effective charge carrier lifetime for the silicon wafer is around 150μs.

suitable for use in real-world applications. Additionally, long charge carrier lifetimes translate into slow switching speeds. Thus, in order to increase photomodulator efficiency whilst maintaining reasonable optical intensities and fast switching speeds one needs to increase the impact of small changes in Δn on the reflection/transmission from/through a modulator. This can be achieved by increasing the light-matter interaction.

The simplest way to increase light-matter interaction is by introducing a Fabry-Perot resonance within the wafer itself. This effect can be seen in Figure 1(a). We have performed calculations using the transfer matrix method to calculate the transmission and reflection modulation for a silicon wafer. Eqn. 1 is used to calculate the charge carrier concentration, and the Drude model used to calculate the permittivity of the silicon based on this. Full details of the simulation can be found in reference[13]. We investigate the effect of the wafer thickness on the modulation, as shown in figure 1(a). In agreement with Eqn. 1, we see that the highest modulation is predicted for the thinnest wafers. However, there is also a clear periodicity in modulation with wafer thickness; when the wafer thickness is equal to an integer number of half-wavelengths in the silicon ($n \times 314\,\mu$m) we see a dip in the modulation of a reflected beam, and a peak in the modulation of a transmitted beam. This is a result of Fabry-Perot modes within the wafer, which increase the light-matter interaction,leading to increased modulation.

In figure 1(b) we present a measurement of the transmission of a 140 GHz beam incident at 45° impinging on a 290μm thick high-resistivity float-zone silicon wafer, i.e. near the 1st Fabry-Perot peak predicted by our model in figure 1(a). We plot this as a function of the intensity of the optical excitation, which is also incident at 45°. The solid line in figure 1(a) shows the results of simulations assuming a lifetime of 150μs (measured for our wafer using a pulsed excitation source and ultrafast detector). The simulation is in reasonable agreement with the experimental results. The small discrepancies can be attributed to an uncertainty ($\pm$1μm) in the thickness of the wafer. The maximum optical intensity incident on the wafer in this study is 0.006 W/cm^2, of which 65.1% is absorbed and 34.9% is reflected. The modulation in transmission with this incident intensity is just less than 10%, and in reflection is around 5%, giving a figure of merit for a reflection modulator of 833 % per W/cm^2. This is already comparable to the modulation FoM given for other cavity-based photomodulators in Table 1[15,16].

In figure 1(c) we present the time-dependent dynamics of this modulator upon switching on the pump beam. Assuming an approximate exponential increase/decrease in carrier density as a function of time after a switch-on/switch off event, our measured 150μs carrier lifetime corresponds to a switching speed of 300μs (the time for the signal to rise and fall

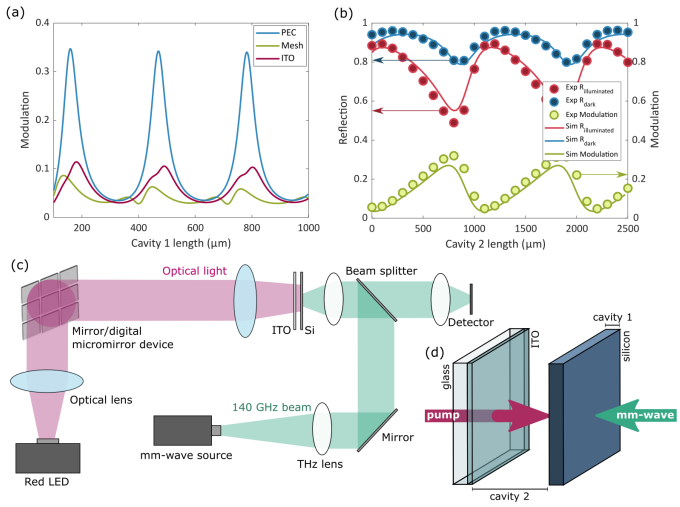

FIG. 2. (a) Calculated modulation of a 140 GHz beam reflected from a silicon wafer (cavity 1) of varying length with a charge carrier lifetime of 150 μs, placed against a reflective layer of perfect electric conductor (PEC), a 10 μm thick copper mesh and a 250 nm thick layer of ITO. The pump beam has a wavelength of 623 nm and an intensity of 0.006 W/cm^2. (b) Experimental (circles) and calculated (solid lines) reflection (left axis) and modulation (right axis) for the coupled-cavity photomodulator as a function of the length of cavity 2 for a normally incident 140 GHz beam when cavity 1 is 290 μm long, and the same pump parameters as above. (c) Schematic of experimental set-up used to measure the data presented in (b). (d) Close up of the coupled-cavity modulator design.

by a factor of 1/e) and an intrinsic maximum modulation rate of approximately 3 kHz. This is considerably faster than the higher efficiency modulators recorded in Table I, and typical of the repetition rates required for many applications (such as single pixel imaging[1,12]). However, the relatively low modulation efficiency of 833 % per W/cm^2 is a drawback. If we would like a modulator that operates at high speed and with very low optical intensities, the modulation offered by a single silicon wafer is somewhat limited. In the following sections we investigate ways to increase the modulation by increasing the quality factor of the Fabry-Perot resonance in the silicon (which we will, from here on, refer to as cavity 1), with a second cavity, cavity 2. We show that this coupled cavity approach can significantly increase the modulation efficiency of our planar modulator.

III. COUPLED-CAVITY DESIGN

We first consider whether improvements to the quality factor of the single cavity can be easily achieved. Large increases in modulation can be obtained when the electric field amplitude of the mm-wave beam we want to modulate is large inside the silicon wafer. For a Fabry Perot cavity, the maximum electric field amplitude inside the cavity, achieved on resonance, is determined by the reflectivity of the interfaces. One option for increasing the effect of cavity 1 is therefore to increase the reflectivity of one (or both) of the wafer interfaces, as shown in ref[16]. Ideally, a layer of a highly conducting metal such as gold or copper would be used for this. However, this is impractical for a photomodulator, as the reflective layer must also be transparent to the pumping light. This suggests two obvious options: 1) a mesh made of highly conducting (e.g. copper) wires, or 2) a layer of optically transparent conductor such as indium tin oxide (ITO). It should be noted that increasing the light-matter interaction within the silicon wafer will not affect the charge carrier lifetime, and hence the rate of operation is not compromised due to the improvements we make throughout this paper.

Figure 2 (a) shows the modulation calculated for each of these cases, compared to the idealised case of a perfect electrical conducting (PEC) layer (which assumes no loss). This is calculated using the same transfer matrix approach as described previously. In each case, a layer of the reflective material is set on the opposite side of the silicon wafer from the incident mm-wave beam. To be realistic, we also assume a substrate for this reflective layer: a 0.7 mm thick layer of glass on the air side of the reflector ($\varepsilon = 3.9 + 0.005i$), and consider an optical excitation of wavelength 623 nm and intensity 0.006 W/cm^2 impinging on the silicon. The largest modulation is predicted for the PEC reflective layer ($\varepsilon = -1 \times 10^6$). However, for realistic, transparent conducting layers this expected enhancement in modulation is almost completely suppressed. The first such case we consider is a fine copper mesh, with a pitch small enough to act as a reflector at mm-wave frequencies, yet large enough to be partially transparent at optical frequencies. Modal matching[22] is used to extract an effective permittivity (-193.7) and permeability (0.51) for a mesh with a pitch of 254 μm, made of wires with a square cross-section of 10 μm width (typical of commercially available meshes) which gives an optical transparency of 81%. Full-wave simulations of various meshes can be found in the supplementary material. For this case, even though this mesh is assumed to have no absorption, the drop in the reflectivity (90%) compared to the PEC is large enough to drastically reduce the modulation predicted for the cavity, as seen in figure 2(a). The second approach we investigate is to employ a transparent conductive layer such as ITO (optical transparency of 89% for a 250 nm thick layer). The ITO permittivity was calculated using the Drude model, with a plasma frequency of 1.65×10^{15} and scattering rate of 1.43×10^{14}, following reference[23], and found to be $-554.3 + 4.4 \times 10^4 i$. While the enhancement in predicted modulation for the ITO case is considerably larger than for the mesh, the enhancement falls well short of the PEC predictions due to high absorptive losses caused by the close proximity of the ITO to the silicon modulator. However, since the ITO shows greater modulation than the copper mesh due to its higher reflectivity, we only consider an ITO reflective layer for the remaining discussion below.

To overcome the loss problem, we introduce an air gap between the ITO reflective layer and the silicon, forming a second cavity between the ITO layer and the silicon wafer, referred to as cavity 2. Figure 2(c) shows a schematic of the experimental set up used to measure the reflection modulation from the coupled-cavity modulator, and Figure 2(d) is a

close up of the modulator design. Further details of the experiment can be found in section 3 of the supplementary material. Cavity 2 provides a second resonance that is coupled to the resonance in cavity 1. This results in a hybrid mode with a resonance frequency that can be simply tuned by adjusting the distance between the ITO and the wafer. In the experiment the silicon wafer is mounted on a translation stage so that the length of cavity 2 can be adjusted with 10 µm precision. Figure 2(c) shows both the measured and modelled reflectivity (left axis) of 140 GHz radiation from a modulator consisting of a 290 µm thick silicon wafer separated from a 250 nm thick layer of ITO on 0.7 mm of glass when illuminated and dark, as well as the resulting modulation (right axis). The solid lines show the results of transfer matrix calculations, as described in the previous section, while the circles are the experimental results. A distinctive periodicity in the reflection is evident, the origin of which is discussed in more detail in the supplementary material. At the optimal length for cavity 2, we can compare the results to figure 1. For an optical intensity of 0.006 W/cm^2, the maximal modulation is found to be 32%, giving a figure of merit of 5333 % per W/cm^2. This is 7 times larger than that of an isolated wafer in reflection, and around 3 times larger than found in the transmission geometry. It is also several orders of magnitude larger than other photomodulators of similar modulation rate (see table I). Furthermore, by introducing the second cavity, we now achieve a modulation close to that predicted for the PEC enclosed single cavity, as presented in figure 2(a).

The coupling between cavities 1 and 2 brings about tuneability that is not present for the wafer alone. This degree of tunability is a significant advantage of our modulator, making it more flexible and tolerant than other approaches. By simply altering the length of cavity 2, one can tune the resonance the resonance frequency of our coupled-cavity modulator to any mm-wave frequency. Figure 3(a) shows the simulated modulation as a function of incident frequency and length of cavity 2 when cavity 1 is 290 µm long, under the same illumination conditions as described previously. It can be seen that changing the length of cavity 2 from 0 to 1 mm will give a modulation that is greater than 30% for resonant frequencies. This resonance enhancement is particularly obvious when both cavity one and cavity 2 are near resonant (120 - 180 GHz), with broad anticrossing features leading to enhanced modulation across broad, fractional bandwidths of up to 40%. Outside of this frequency range, resonance features are much narrower, and modulation is lower than for the doubly resonant region.

We also predict that the broad enhancement effects are relatively angle independent. This is very important for some spatial modulation applications (such as imaging with a high numerical aperture), where a constant modulation over a range of angles is required. Figures 3(b) and (c) show the modulation as a function of the length of cavity 2 and incident angle for a frequency of 140 GHz for TE and TM polarised beams, respectively. For the lowest order mode, found at a length of cavity 2 of approximately 600 µm at normal incidence, the modulation is relatively constant for both polarisations for incident angles up to $\sim 40^\circ$, corresponding to a numerical aperture of ~ 0.65 in air. For angles beyond this, we observe some interesting features in our calculations: for a TE polarised beam beyond 40° the modulation increases beyond that achieved at normal incidence. This is due to the increase in reflectivity of the air-silicon interface upon increasing incident angle. The opposite is true for a TM polarised wave, which experiences a decrease in the reflectivity of the interface as the angle approaches the Brewster angle (73.6°). However, we note that at these higher angles of incident the tunability with cavity length is much reduced, and the angular dispersion increased, potentially limiting the range of applications where this increase in modulation could be utilised.

IV. CONCLUSIONS AND FUTURE WORK

In conclusion, we have designed and tested a highly efficient mm-wave photomodulator by coupling the resonant Fabry-Perot modes in two cavities - one in a silicon wafer and one in an air-gap between the wafer and a transparent conductor, in this case ITO. This photomodulator design was tested experimentally, and found to give a modulation in reflection that is a factor of 7 larger than that achievable with an isolated silicon wafer; 32% for an optical excitation of only 0.006 W/cm^2. We also find that tuning the length of the cavity between the wafer and reflector can result in modulations of more than 30% over a range of frequencies between 120 GHz and 180 GHz, and that the modulation is relatively constant for incident angles up to 40° from normal.

Due to the low angular dispersion, our enhanced modulator approach is particularly useful when spatial modulation is required, as in single pixel imaging or spatial encoding of information in communication networks. Since the modulation is enhanced by the cavities, one can achieve good modulation for relatively low light intensities and for silicon with relatively short electron-hole lifetimes. This will increase the spatial fidelity of patterned modulation while maintaining high contrast and high amplitude modulation, as shown in the inset in figure 3 (c). While we apply this design approach to optimise a 3KHz modulator suitable for many applications such as single pixel imaging[1,12], we also note that the same principals can be applied to also enhance significantly faster modulators. We believe this highly efficient but simple design strategy can therefore be an important step towards the real-world application of THz and mm-wave technologies.

SUPPLEMENTARY MATERIAL

See the supplementary material for further details of the experimental design, the analysis of the mesh-wall cavities and a more in-depth discussion of the nature of the coupled modes.

ACKNOWLEDGMENTS

The authors wish to thank Dr. Dave Phillips for his contributions to the paper, as well as Dr. John Murphy and Dr.

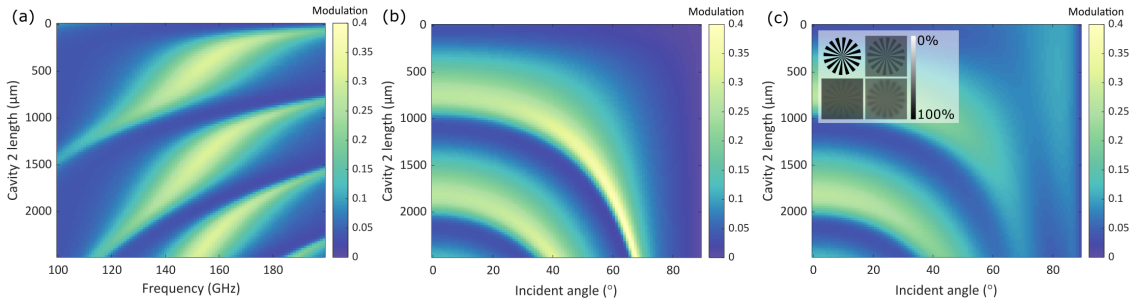

FIG. 3. (a) Calculated modulation at normal incidence as a function of the frequency and length of cavity 2 when cavity 1 is 290 μm long, and the silicon has an effective charge carrier lifetime of 150 μs. The pump beam has a wavelength of 623 nm and intensity of 0.006 W/cm^2. (b) Modulation of a TE polarised 140 GHz beam as a function of incident angle and length of cavity 2 when cavity 1 is as described above. (c) Equivalent plot for a TM polarised beam. Inset: the simulated contrast and blurring due to diffusion of charge carriers of a patterned modulation with, clockwise from top left, the original, our 150 μs lifetime wafer in the cavity, a 6900 μs lifetime wafer without the cavity, and a 150 μs lifetime wafer without the cavity.

Nick Grant for their advice. L.E.B and I.R.H. acknowledge financial support from the Engineering and Physical Sciences Research Council of the United Kingdom (EPSRC UK) and QinetiQ Ltd. via the TEAM-A Prosperity Partnership (Grant No. EP/R004781/1). E.H. acknowledges financial support from the EPSRC UK (Grant No. EP/S036466/1) and the EPSRC UK (Grant No. QuantIC EP/M01326X/1).

DATA AVAILABILITY

The data that support the findings of this study are available from the corresponding author upon reasonable request.

[1] G. M. Gibson, B. Sun, M. P. Edgar, D. B. Phillips, N. Hempler, G. T. Maker, G. P. A. Malcolm, and M. J. Padgett, "Real-time imaging of methane gas leaks using a single-pixel camera," Optics Express **25**, 2999 (2017).

[2] D. Shrekenhamer, C. M. Watts, and W. J. Padilla, "Terahertz single pixel imaging with an optically controlled dynamic spatial light modulator," Optics Express **21**, 12507 (2013).

[3] R. I. Stantchev, J. C. Mansfield, R. S. Edginton, P. Hobson, F. Palombo, and E. Hendry, "Subwavelength hyperspectral THz studies of articular cartilage," Scientific Reports **8**, 1–8 (2018).

[4] J. Federici and L. Moeller, "Review of terahertz and subterahertz wireless communications," Journal of Applied Physics **107** (2010), 10.1063/1.3386413.

[5] S. Koenig, D. Lopez-Diaz, J. Antes, F. Boes, R. Henneberger, A. Leuther, A. Tessmann, R. Schmogrow, D. Hillerkuss, R. Palmer, T. Zwick, C. Koos, W. Freude, O. Ambacher, J. Leuthold, and I. Kallfass, "Wireless sub-THz communication system with high data rate," Nature Photonics **7**, 977–981 (2013).

[6] R. Singh, A. K. Azad, Q. X. Jia, A. J. Taylor, and H.-T. Chen, "Thermal tunability in terahertz metamaterials fabricated on strontium titanate single-crystal substrates," Optics Letters **36**, 1230 (2011).

[7] B. Jafari, H. Soofi, and K. Abbasian, "Low voltage, high modulation depth graphene THz modulator employing Fabry–Perot resonance in a metal/dielectric/graphene sandwich structure," Optics Communications **472**, 125911 (2020).

[8] Y. Zhang, S. Qiao, S. Liang, Z. Wu, Z. Yang, Z. Feng, H. Sun, Y. Zhou, L. Sun, Z. Chen, X. Zou, B. Zhang, J. Hu, S. Li, Q. Chen, L. Li, G. Xu, Y. Zhao, and S. Liu, "Gbps terahertz external modulator based on a composite metamaterial with a double-channel heterostructure," Nano Letters **15**, 3501–3506 (2015).

[9] B. Sensale-Rodriguez, R. Yan, M. M. Kelly, T. Fang, K. Tahy, W. S. Hwang, D. Jena, L. Liu, and H. G. Xing, "Broadband graphene terahertz modulators enabled by intraband transitions," Nature Communications **3** (2012), 10.1038/ncomms1787.

[10] H. T. Chen, W. J. Padilla, M. J. Cich, A. K. Azad, R. D. Averitt, and A. J. Taylor, "A metamaterial solid-state terahertz phase modulator," Nature Photonics **3**, 148–151 (2009).

[11] M. Rahm, J. S. Li, and W. J. Padilla, "THz wave modulators: A brief review on different modulation techniques," Journal of Infrared, Millimeter, and Terahertz Waves **34**, 1–27 (2013).

[12] R. I. Stantchev, B. Sun, S. M. Hornett, P. A. Hobson, G. M. Gibson, M. J. Padgett, and E. Hendry, "Noninvasive, near-field terahertz imaging of hidden objects using a single-pixel detector," Science Advances **2** (2016), 10.1126/sciadv.1600190.

[13] I. R. Hooper, N. E. Grant, L. E. Barr, S. M. Hornett, J. D. Murphy, and E. Hendry, "High efficiency photomodulators for millimeter wave and THz radiation," Scientific Reports **9**, 1–10 (2019).

[14] J.-s. Li and M.-s. Hu, "Enhancement of silicon modulating properties in the THz range by YAG-Ce coating," Scientific Reports **10**, 6605 (2020).

[15] T. Chen, P. Liu, J. Liu, and Z. Hong, "A terahertz photonic crystal cavity with high Q-factors," Applied Physics B: Lasers and Optics **115**, 105–109 (2014).

[16] N. Born, M. Scheller, M. Koch, and J. V. Moloney, "Cavity enhanced terahertz modulation," Applied Physics Letters **104** (2014), 10.1063/1.4868416.

[17] Q.-y. Wen, Y.-l. He, Q.-h. Yang, P. Yu, Z. Feng, W. Tan, T.-l. Wen, Y.-x. Zhang, Z. Chen, and H.-w. Zhang, "High-Performance Photo-Induced Spatial Terahertz Modulator Based on Micropyramid Silicon Array," Advanced Materials Technologies **1901058**, 1–8 (2020).

[18] T. Wen, J. Tong, D. Zhang, Y. Zhu, Q. Wen, Y. Li, H. Zhang, Y. Jing, and Z. Zhong, "Semiconductor terahertz spatial modulators with high modulation depth and resolution for imaging applications," Journal of Physics D: Applied Physics **52** (2019), 10.1088/1361-6463/ab146d.

[19] X. Liu, E. P. Parrott, B. S. Ung, and E. Pickwell-MacPherson, "Exploiting total internal reflection geometry for efficient optical modulation of terahertz light," APL Photonics **1**, 076103 (2016).

[20] Q. Sun, X. Chen, X. Liu, R. I. Stantchev, and E. Pickwell-MacPherson, "Exploiting Total Internal Reflection Geometry for Terahertz Devices and Enhanced Sample Characterization," Advanced Optical Materials **8**, 1–15 (2020).

[21] Q. Y. Wen, W. Tian, Q. Mao, Z. Chen, W. W. Liu, Q. H. Yang, M. Sanderson, and H. W. Zhang, "Graphene based all-optical spatial terahertz modulator," Scientific Reports **4**, 2–6 (2014).

[22] E. K. Stone and E. Hendry, "Dispersion of spoof surface plasmons in open-ended metallic hole arrays," Physical Review B - Condensed Matter and Materials Physics **84**, 1–9 (2011).

[23] C. W. Chen, Y. C. Lin, C. H. Chang, P. Yu, J. M. Shieh, and C. L. Pan, "Frequency-dependent complex conductivities and dielectric responses of indium tin oxide thin films from the visible to the far-infrared," IEEE Journal of Quantum Electronics **46**, 1746–1754 (2010).